

## Monte Carlo modelling of a NaI(Tl) scintillator detectors using MCNP simulation code

I. Mouhti<sup>1</sup>, A. Elanique<sup>1,\*</sup>, M. Y. Messous<sup>2</sup>

1. Faculty of Sciences, Laboratory of Condensed Matter Physics and Nanomaterials for Renewable Energy, BP 8106, University Ibn Zohr, 80000 Agadir, Morocco

2. National Center for Energy, Sciences and Nuclear Techniques  
-CNESTEN-B.P 1382 R.P 10001, Rabat, Morocco

Received 22 Sep 2016,  
Revised 03 Jan 2017,  
Accepted 13 Jan 2017

### Keywords

- ✓ Monte Carlo simulation;
- ✓ MCNP code;
- ✓ NaI detector;
- ✓ Absolute efficiency;
- ✓ Gamma-ray spectrometry

A Elanique  
[elanique01@yahoo.com](mailto:elanique01@yahoo.com)

### Abstract

Due to their attractive performances, inorganic scintillators such as NaI(Tl) detectors are widely used in the field of gamma-ray spectrometry where knowledge of detector efficiency is a key factor for successful quantitative  $\gamma$  ray analysis. Monte Carlo simulations using MCNP code have been performed in order to evaluate absolute efficiency of NaI detectors. Two mathematical models were constructed for the NaI crystal: 7.62cm x 7.62cm cylindrical NaI and 7.62cm diameter spherical NaI. Detector efficiency was calculated for both NaI detectors in the photon energy range from 60 keV to 2750 keV. Simulation results were compared to experimental efficiency data.

## 1. Introduction

Inorganic scintillators such as NaI(Tl) crystals are widely used for the detection of ionizing radiations, especially gamma rays. This is firstly due to the high atomic number of its iodine constituent ( $Z=53$ ) which assures that photoelectric absorption will be a relatively important process [1]. Other interesting performances of such attractive material are their simplicity of use at room temperature (no cryogenic system required), robustness and relatively low cost.

Knowledge of detector efficiency is absolutely essential when performing quantitative  $\gamma$  ray analysis using a gamma spectrometry. Detector efficiency is described either as “absolute”,  $\epsilon_a(E)$ , or “intrinsic”,  $\epsilon_i(E)$ , where  $E$  is the absorbed photon energy. Absolute efficiency is the product of  $(\Omega/4\pi)$  and the intrinsic efficiency of the detector, whereas  $(\Omega/4\pi)$  denotes the fractional solid angle subtended by the detector at point source position [2]. Intrinsic efficiency is the probability that a photon incident on the detector will produce a recorded pulse. For NaI scintillators,  $\epsilon_i(E)$  mostly depends on the crystal dimensions, the thickness of Aluminium housing material and other absorbing layers like MgO reflector. The detector efficiency is commonly measured by calibration sources or computed by Monte Carlo (MC) simulations.

Since the advent of fast and low-cost personal computers, mathematical modelling of radiation detectors using Monte Carlo (MC) programs is becoming a powerful and convenient tool to fully characterize detector parameters by simulating the transport of radiation through matter. The Monte Carlo methods make it possible to calculate the response function for detectors with good accurate results [3, 4].

In the work reported here, the MCNP code [5], based on the Monte Carlo method, was used to evaluate the photon detection efficiency for a 7.62cm x 7.62cm NaI(Tl) scintillator detector in the 60-2750 keV photon energy range. We simulated two geometrical configurations for the NaI crystal: cylindrical and spherical. In both cases, the detector was exposed to gamma rays from 4 radioactive isotropic point like sources:  $^{241}\text{Am}$ ,  $^{137}\text{Cs}$ ,  $^{22}\text{Na}$ ,  $^{60}\text{Co}$  and  $^{54}\text{Mn}$ .

## 2. Monte Carlo simulations

### 2.1. Monte Carlo code

The simulations were performed using the Monte Carlo (MC) code MCNP version 4C to calculate the NaI detector efficiency. This code is a general purpose radiation transport code developed at the Los Alamos National Laboratory. It is used to calculate coupled neutron-photon-electron transport. For photons, MCNP accounts for Compton scattering (incoherent) and Thomson scattering (coherent), the possibility of fluorescent

emission after photoelectric absorption, and pair production with local emission of annihilation radiation, and *bremstrahlung*. The code obtains the solution of the problem by simulating individual particle trajectories and recording some aspects of their average behaviour (it does not solve the Boltzmann particle transport equation). The individual probabilistic events that comprise a process of interaction of nuclear particle with material are sequentially simulated. Each particle may generate additional particles (daughters) or tracks at a collision site. Each history (birth to death) is considered an independent random event.

MCNP is immediately suitable for modelling the detector response, since it contains a special tally, F8, which is specific for pulse height determination, i.e. energy deposited in the detector. Thus, the pulse-height tally per photon emitted from the source gives the absolute efficiency  $\epsilon_a(E)$  for each spectral peak in the chosen geometry. In the MCNP code, the tracking of each photon, as well as each photon and electron resulting from interactions in the detector, is followed until its energy in the detector is low enough for it to be considered “killed” (1 keV cutoff).

### 2.2. Accuracy versus precision of the MCNP results

To understand the precision and acceptability of the tally results produced by the Monte Carlo run, we should distinguish between precision and accuracy of MC results.

The *Accuracy* is a measure of how close the result is to the “true” physical quantity being estimated. When running a MC calculation, many factors can significantly affect the accuracy of the results. This includes inaccuracies introduced by MCNP in its use of (1) physics models, (2) uncertainties in the photon cross sections (<2%) over the considered energy range [6] and (3) eventually poor modelling of the actual detector geometry by the MC simulations. Indeed, the detector specifications, generally provided by the manufacturer, are often not sufficient and sometimes need to be optimised by radiographic imaging [3, 4, 7].

By contrast, *precision* of the MC method is the statistical counting error caused by the statistical fluctuations ( $\sigma \sim 1/\sqrt{N}$ ), where  $N$  is the number of particles histories considered. The more histories run, the better will be the precision of the tallies [8].

In the present work, the number of particles histories simulated in each run was  $10^6$  so that the precision of the MC results was always kept below 0.2%. MC simulations were performed using MCNP with default physics features enabled and detailed tracking of both photons and electron (i.e. *mode p e*).

### 2.3. Modelling the NaI detector

Two mathematical models for the NaI detectors were constructed using MCNP4C code: a) cylindrical 7.62cm x 7.62cm model [9] and b) spherical 7.62cm x 7.62cm model [10]. The inner structure of the studied NaI detectors is shown in Figure 1.

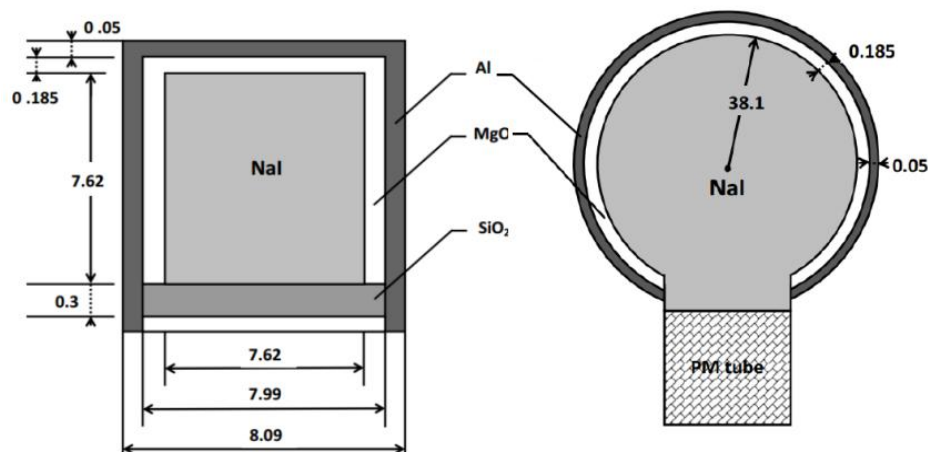


**Figure 1:** Cross section of the MCNP detector models. The spherical NaI detector (right) and the cylindrical one (left) are represented. Distances are in *mm*.

The NaI crystal density was  $3.667 \text{ g.cm}^{-3}$ , the MgO reflector density was  $2 \text{ g.cm}^{-3}$  [11] and the aluminium density was  $2.7 \text{ g.cm}^{-3}$ . The estimated weight of the crystal volume in the spherical model ( $\sim 850 \text{ g}$ ) was in agreement with the value of 847 g from [10]. This confirms the exactness of the actual model used for the spherical detector.

To account for backscattering, the window of the PM tube was modelled as being composed from glass ( $\text{SiO}_2$  layer), having an effective density of  $0.94 \text{ g.cm}^{-3}$ . Nevertheless in the present study this layer did not play a

significant role since it was located in the backside of the NaI crystal. All gamma ray emitting sources were modelled as point “like” isotropic sources. They were placed 10 cm from the detector surface on the centre axis. The full energy peak in the simulated spectra was treated as a Gaussian peak whose resolution ( $\Delta E$ ) i.e. Full Width at Half Medium (*FWHM*) was derived from the measured photopeak [12]. This broadening is required to take into account the statistical fluctuations in each step during pulse creation process. Among these are the following: efficiency of light collection and transfer of photons to photocathode (NaI sensitive volume), charge multiplication in the dynode structure (PM) and pulse amplification (electronics). It should be noted that the MC code does not account for all these effects that would contribute to the observed width.

The Gaussian energy broadening (GEB) option was used to simulate the statistical variance in the photopeak centred at energy  $E$  (MeV). In MCNP4C code, this broadening is defined by the (*FWHM*) or  $\Delta E$ :

$$FWHM = a + b\sqrt{E} + cE^2$$

Where constants  $a$ ,  $b$  and  $c$  are equal to -0.0137, 0.0752, and -0.1210 respectively.

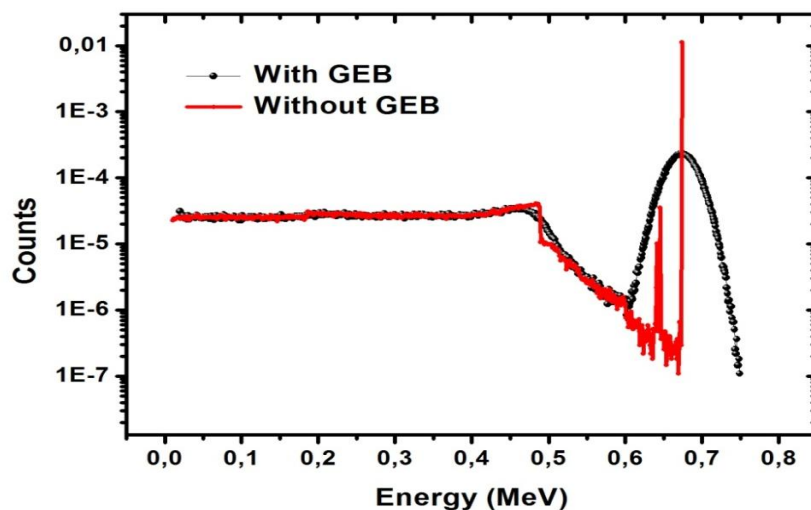


**Figure 2:** Pulse height distribution (PHD) of  $^{137}\text{Cs}$  simulated by MCNP for a cylindrical NaI detector. The graph illustrates the effect of Gaussian energy broadening (GEB) option on the full energy peak. The spectral line at 662 keV represents the full energy peak while the peaks centred at  $\sim 634$  keV are attributed to Iodine x-rays escape (see page 331 of [1]).

The effect of broadening the photopeak is better illustrated in Figure 2 where the Pulse Height Distribution (PHD) of  $^{137}\text{Cs}$  point source is simulated for a cylindrical 7.62cm x 7.62cm NaI detector with and without GEB option (i.e. GEB option turned on/off). Typically, for a 7.62cm x 7.62cm NaI cylindrical detector the energy resolution ( $FWHM/E$ ) at 662 keV energy is about 6-7% (see page 347 of [1]).

### 3. Results and Discussion

All MC generated spectra were normalized to the highest measured value in the mean channel of the full energy peak. Results from MCNP4C simulations are shown in Figure 3 which represents the PHD of a cylindrical 7.62cm x 7.62cm NaI detector for 200 keV photons. The obtained spectrum does not consider the effects of GEB (which is the default option in the MCNP code). The spectral line (full energy peak) at 200 keV was reduced by a factor of 100 for better viewing. The peak centred at  $\sim 172$  keV is attributed to Iodine K x-rays escape from the surface of the NaI crystal [13]. When this occurs, the energy of the x-ray (28 keV) is lost. The Compton continuum can be clearly identified below  $\sim 70$  keV.

A comparison between empirical and MCNP4C simulated spectra of the cylindrical NaI(Tl) detector in the case of (a)  $^{137}\text{Cs}$  and (b)  $^{60}\text{Co}$  sources is shown in Figure 4. The plotted measurement data points were reproduced from [9], whereas MCNP4C simulation indicates present work. A good agreement between simulated and measured energy spectra for both “point” sources can be seen.

While for the  $^{137}\text{Cs}$  source the measured and MC calculated spectra match well, for the  $^{60}\text{Co}$  source however we observe a systematic difference in the Compton continuum below 600 keV. This is most likely due to non-proportional scintillation efficiency of the NaI crystals at low energy region [14]. The latter which is defined as the light output per unit deposited energy, is not a constant value and is not considered in the MCNP4C code.

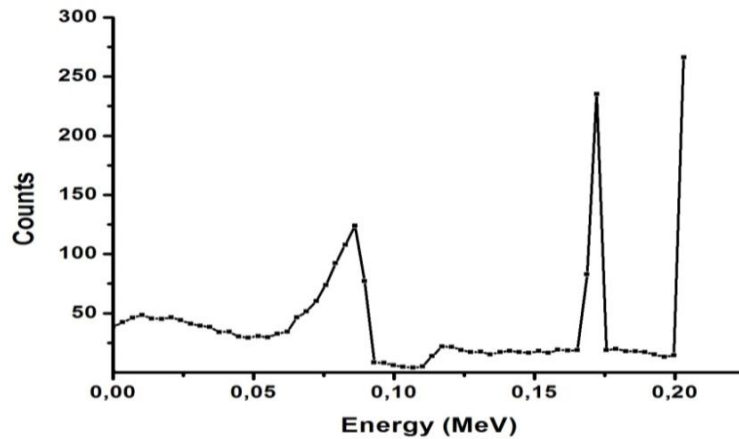


**Figure 3:** Pulse height distribution generated by MCNP code for the spherical NaI detector at 200 keV photons. For better viewing, the full energy peak was reduced by a factor of  $\sim 100$ . The Iodine K x-rays escape peak ( $\sim 172$  keV [13]) and the Compton edge below ( $\sim 70$  keV) can be clearly identified.

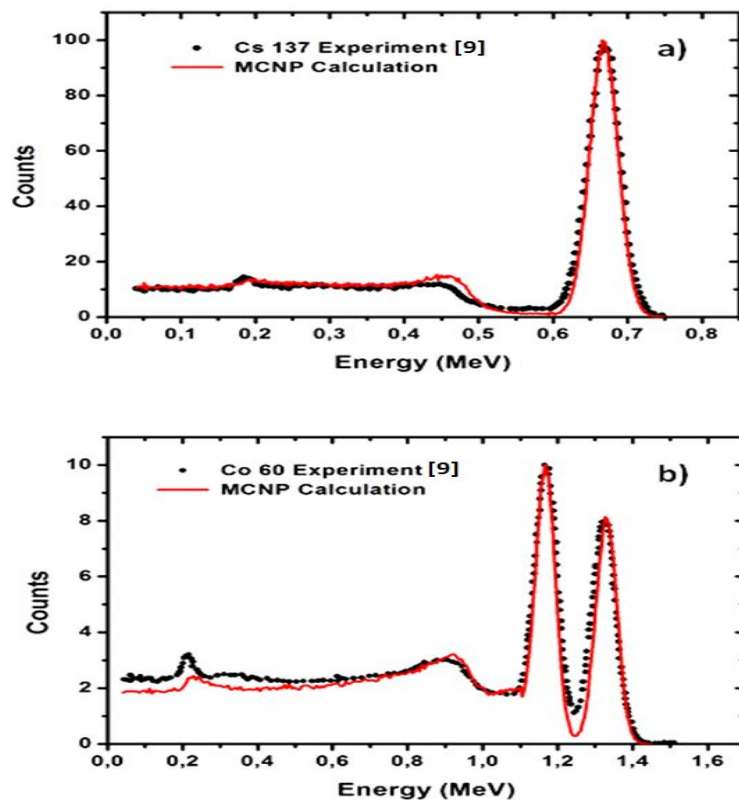


**Figure 4:** Comparison between empirical and simulated spectra of the cylindrical NaI (Tl) detector in the case of (a)  $^{137}\text{Cs}$  and (b)  $^{60}\text{Co}$  sources. The two point isotropic sources were placed on the center axis of the detector at 10 cm from the detector face. Data were from ref. [9], while MCNP calculations correspond to present work.

It should be noted that the “backscatter peak” of Figure 4 in the vicinity of 0.2-0.25 MeV energy region was not reproduced by MC simulations. This peak arises from Compton scattering of gamma rays in the walls of the shield surrounding the detector [15]. The reason is that the actual MC model simulates only the detector-source system rather than the whole experimental setup including the shield.

In table 1, MC simulated efficiencies are compared to measured values for both NaI detector models (cylindrical and spherical) in the photon energy range 60 keV-2750 keV. The relative error of the measured efficiencies was reported to be ( $\sim 2.5\%$ ) in the spherical NaI detector [10]. The uncertainty of the MC results was about 5%. Recall that for the cylindrical NaI detector, uncertainties on efficiency data were not provided in [9]. The results presented in table 1 indicate that the Monte Carlo efficiencies for the studied NaI detectors agreed well with the measured values. Nevertheless, for the cylindrical NaI detector, we observed a significant difference between MC values and efficiency data in particularly for the  $^{60}\text{Co}$  gamma energies (1173 and 1332 keV) and similarly

for  $^{22}\text{Na}$  photon energy at 1272 keV: The measured efficiencies are about 47% lower than the MCNP values in the  $^{60}\text{Co}$  case and about 10% lower in the  $^{22}\text{Na}$ . The origin of these discrepancies would be attributed to the larger uncertainties in the experimental efficiencies. Indeed, when re-observing the experimental  $^{60}\text{Co}$  spectrum of figure 4 b), the two peaks are poorly separated (at such energy, NaI energy resolution is about ~12%) and consequently a bad subtracting of the Compton background from the two peaks results in both a wrong net count as well as an inaccurate efficiency determination.

**Table 1:** NaI(Tl) detector's efficiency values obtained by MC simulation and measurements. Sources were located at 10 cm from the face of the detector. Efficiency data were from [10] for the spherical NaI detector and from [9] for the cylindrical NaI detector. For the spherical NaI detector, efficiency data corresponding to  $^{22}\text{Na}$ ,  $^{54}\text{Mn}$  and  $^{241}\text{Am}$  sources were not given (n.g.)

Source	Photon energy (KeV)	Cylindrical NaI detector		Spherical NaI detector	
		Measured	MCNP	Measured	MCNP
$^{241}\text{Am}$	60	n.g.	2.83	n.g.	1.271±0.001
$^{22}\text{Na}$	510.6	1.431	1.435		
	1272.7	0.590	0.649		
$^{24}\text{Na}$	2754	n.g.	0.329	n.g.	0.191±0.006
$^{54}\text{Mn}$	834.7	0.812	0.861		
$^{137}\text{Cs}$	661.7	1.07	1.04	0.684±0.01	0.690±0.02
$^{60}\text{Co}$	1173.2	0.470	0.698	0.416±0.01	0.415±0.01
	1332.5	0.455	0.625	0.369±0.008	0.370±0.02

## Conclusion

In the present work, Monte Carlo simulations of a two NaI(Tl) detectors using MCNP4C code were performed. Two mathematical models were constructed for the NaI crystal: 7.62cm x 7.62cm cylindrical NaI and 7.62cm diameter spherical NaI. Detector efficiency was calculated for both NaI detectors in the photon energy range from 60 keV to 2750 keV. The resulting overall agreement between MC efficiency values and empirical efficiency values shows that the MCNP4C code can be successfully used for modelling response functions of these two NaI(Tl) scintillators.

## References

1. Knoll G.F. Radiation detection and measurement, John Wiley & Sons, New York (2000).
2. Johansson S.A.E., Campbell J.L. PIXE—A Novel Technique For Elemental Analysis, John Wiley & Sons, New York (1988).
3. Mesradi M., Elanique A., Nourreddine A., Pape A., Raiser D. *Appl. Radiat. Isot.* 66 (2008) 780.
4. Elanique A., Marzocchi O., Leone D., Hegenbart L., Breustedt B., Oufni L. *Appl. Radiat. Isot.* 70 (2012) 538.
5. Briesmeister J.F. MCNP: A General Monte Carlo N-Particle Transport Code, Version 4C, LA-13709-M, Los Alamos National Laboratory (2000).
6. Hubbell J.H. *Phys. Med. Biol.* 44 (1999) R1.
7. Boson J., Agren G., Johansson L. *Nucl. Instr. Meth., A* 587 (2008) 304.
8. Shultis J. K., Faw R. E. An Mcnp Primer, Kansas state university, USA (2004).
9. Akkurt I., Tekin H.O., Mesbahi A. *Acta Physica Polonica A*, Vol. 128 (2015) B332.
10. Chul-Young Yi, Suck-Ho Hah *Appl. Radiat. Isot.* 70 (2012) 2133.
11. Saito K., Moriuchi S. *Nucl. Instrum. Methods* 185 (1981) 299.
12. Shi H.X., Chen B.X., Li T.Z., Yun D. *Appl. Radiat. Isot.* 57 (2002) 517.
13. Heath, R.L. Scintillation Spectrometry Gamma-Ray Spectrum Catalogue, IDO-16880, vols 1 and 2 AEC Research and Development Report, Physics (updated Feb. 1997) 11.
14. Zerby C.D., Meyer A., Murray R.B. *Nucl. Instrum. Methods* 12 (1961) 115.
15. Berger M. J.; Seltzer S. M. *Nucl. Instr. Meth.* 104 (1972) 317.

(2017) ; <http://www.jmaterenvirosci.com/>